

Viscosity-sensitive and AIE-active bimodal fluorescent probe for the selective detection of OCl^- and Cu^{2+} : a dual sensing approach *via* DFT and biological studies using green gram seeds

Malavika S Kumar^a, Vishnu S^a, Malay Dolai^b, Anish Nag^c, Yatheesharadhya bylappa^c, Avijit Kumar Das^{*a}

^aDepartment of Chemistry, CHRIST (Deemed to be University), Hosur Road, Bangalore, Karnataka, 560029 India, Email: avijitkumar.das@christuniversity.in

^bDepartment of Chemistry, Prabhat Kumar College, Contai, Purba Medinipur 721404, W.B., India

^d Department of Life Science, CHRIST (Deemed to be University), Hosur Road, Bangalore, Karnataka, 560029

CONTENTS

1. General methods of UV-vis and fluorescence titration experiments	1
2. Association constant determination.....	2-3
3. Determination of fluorescence quantum yields.....	3
4. Calculation of the detection limit.....	4
5. Job's plot analysis.....	5
6. DLS analysis.....	5
7. Rate constant calculation.....	6
8. ¹ H NMR and Mass spectrum of NCP.....	7
9. ¹³ C-NMR and IR spectrum of NCP.....	8
10. ¹ H-NMR analysis of NCP and NCP + OCl^-	9
11. Mass spectra of NCP + OCl^- and NCP + Cu^{2+}	9
12. Computational details.....	10
13. Comparison table of NCP with the reported similar type of chemosensors.....	11
14. References.....	12

General method of UV-vis and fluorescence titration:

By UV-vis method:

For UV-vis titrations, a stock solution of the sensor was prepared ($c = 2 \times 10^{-5}$ M) in a CH₃CN-HEPES buffer (9/1, v/v, 25°C) at pH 7.4. Solutions of the guest interfering analytes, such as Cl⁻, CH₃COO⁻, Br⁻, F⁻, NO₂⁻, C₂O₄²⁻, NO₃⁻, SO₄²⁻, H₂O₂, Al³⁺, Cd²⁺, Fe³⁺, Fe²⁺, Hg²⁺, Mn²⁺, Cu²⁺, Ni²⁺, Pb²⁺, and Zn²⁺, were also prepared in the order of $c = 2 \times 10^{-4}$ M. Solutions of different concentrations containing sensors and increasing concentrations of cations were prepared separately. The spectra of these solutions were recorded by means of UV-vis methods.

General procedure for drawing Job's plot by UV-vis method:

A stock solution of the same concentration of NCP and Cu²⁺ was prepared in the order of $\approx 2.0 \times 10^{-5}$ M in a CH₃CN-HEPES buffer (9/1, v/v, 25°C) at pH 7.4. The absorbance in each case with different *host-guest* ratios but equal volumes was recorded. Job plots were drawn by plotting $\Delta I \cdot X_{\text{host}}$ vs X_{host} (ΔI = change in the intensity of the absorbance spectrum during titration and X_{host} is the mole fraction of the host in each case, respectively).

By fluorescence method:

For fluorescence titrations, a stock solution of the sensor ($c = 2 \times 10^{-5}$ M) was prepared for the titration of cations and anions in a CH₃CN-HEPES buffer (9/1, v/v, 25°C) at pH 7.4. Solution of the guest cations and anions in the order of 2×10^{-4} M were also prepared. Solutions of different concentrations containing sensors and increasing concentrations of cations and anions were prepared separately. The spectra of these solutions were recorded by means of fluorescence methods.

Association constant determination:

The binding constant value of cation Cu²⁺ with the sensor was determined from the emission intensity data following the modified Benesi-Hildebrand equation, $1 / \Delta I = 1 / \Delta I_{\text{max}} + (1 / K[C]) (1 / \Delta I_{\text{max}})$, where K is the binding constant, $[C]$ is the guest concentration, $\Delta I = I - I_{\text{min}}$ and $\Delta I_{\text{max}} = I_{\text{max}} - I_{\text{min}}$, in which I_{min} , I , and I_{max} are the emission intensities of the sensor considered in the absence of the guest, at an intermediate concentration and at a concentration of complete saturation of the guest. From the plot of $(I_{\text{max}} - I_{\text{min}})/(I - I_{\text{min}})$ against $[C]^{-1}$ for the sensor, the value of K was determined from the slope. The association constant (K_a) as determined by the fluorescence titration method for the sensor with Cu²⁺ was found to be $1.66 \times 10^3 \text{ M}^{-1}$ (error < 10%).

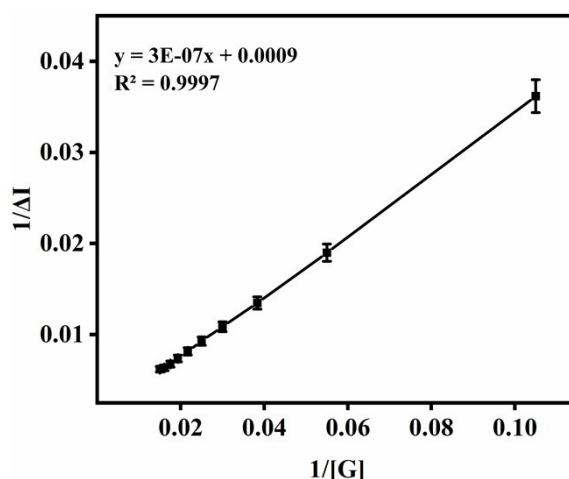


Fig. S1: Benesi–Hildebrand plot from fluorescence titration data of receptor **NCP** ($c = 2.0 \times 10^{-5}$ M) with Cu^{2+} including error bars (error amount, 5%; Y error bar for both $[\pm]$ deviation).

Determination of fluorescence quantum yields:

Here, the quantum yield ϕ was measured using the following equation:

$$\phi_x = \phi_s (F_x / F_s)(A_s / A_x)(n_x^2 / n_s^2)$$

where

X and S indicate the unknown and standard solutions, respectively, ϕ is the quantum yield, F is the area under the emission curve, A is the absorbance at the excitation wave length, and n is the index of refraction of the solvent. Here ϕ measurements were performed using anthracene in ethanol as the standard [$\phi = 0.27$] (error $\sim 10\%$)

Calculation of the detection limit:

The detection limit (DL) of **NCP** for OCl^- and Cu^{2+} was determined using the following equation:

$$DL = K * Sb_1 / S$$

where $K = 2$ or 3 (we take 3 in this case), Sb_1 is the standard deviation of the blank solution, and S is the slope of the calibration curve.

From the graph shown in Fig. S2, we get a slope value of 1.091 , and the Sb_1 value is 1.4464

From the graph shown in Fig. S3, we get a slope value of 38.797 , and the Sb_1 value is 7.0684 .

Thus, using the formula we get the detection limit for Cu^{2+} as $3.97 \mu\text{M}$ and for OCl^- as $0.55 \mu\text{M}$.

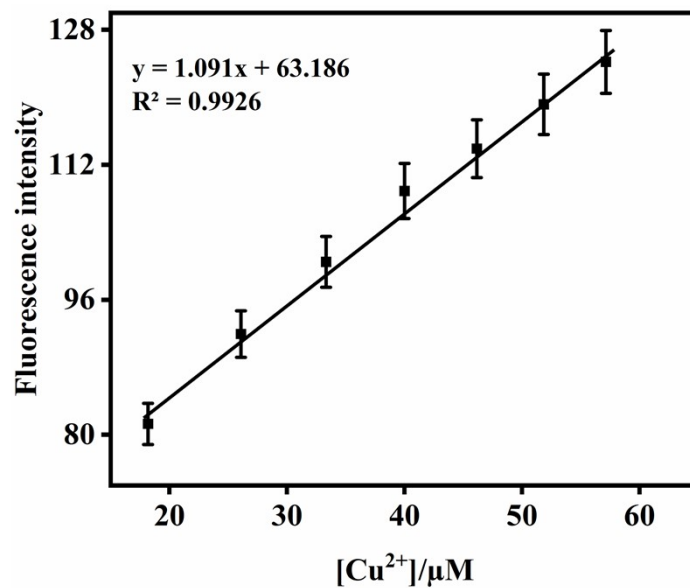


Fig. S2: Changes in the fluorescence intensity of NCP as a function of [Cu²⁺], including error bars (error amount, 5%; Y error bar for both [\pm] deviation).

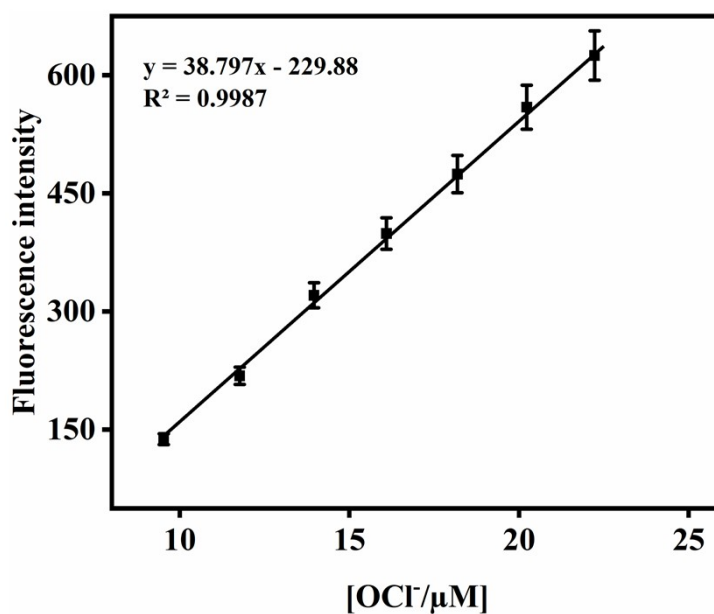


Fig. S3: Changes in the fluorescence intensity of NCP as a function of [OCl⁻], including error bars (error amount, 5%; Y error bar for both [\pm] deviation).

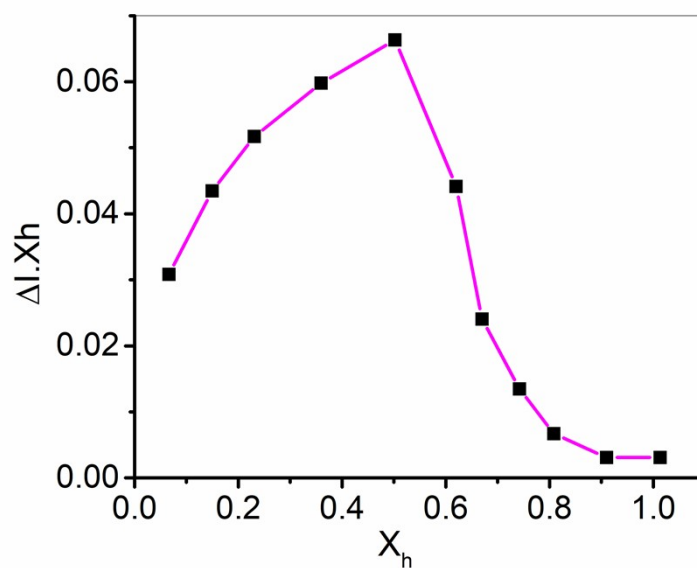


Fig. S4. Job plot diagram of receptor **NCP** for Cu^{2+} (where X_h is the mole fraction of the host and ΔI indicates the change in the intensity).

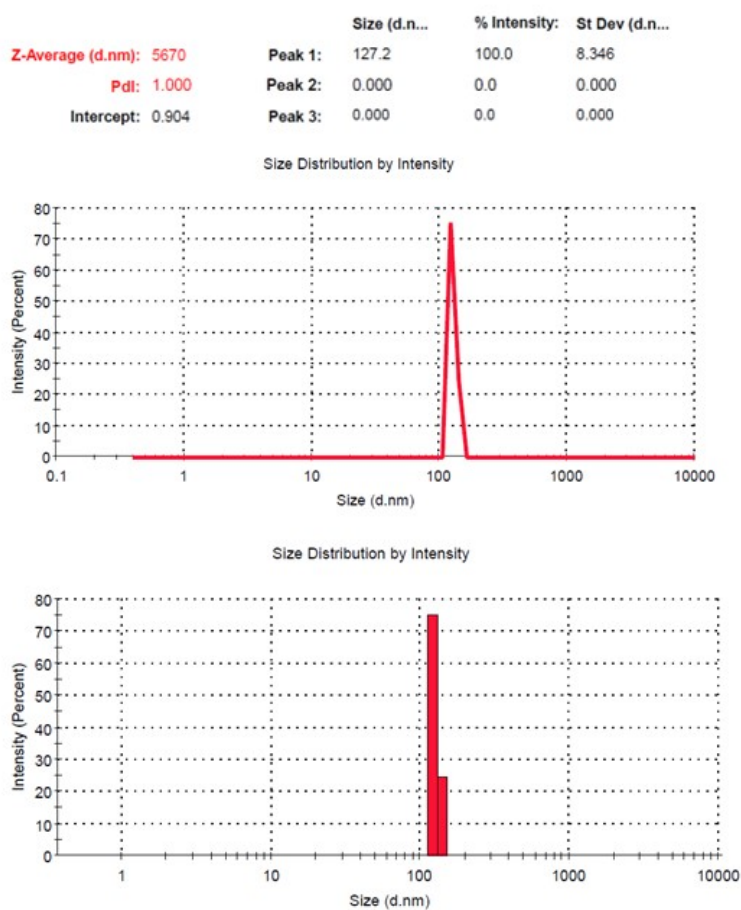


Fig. S5. Results of DLS analysis of **NCP** in $\text{CH}_3\text{CN} : \text{H}_2\text{O}$ (9 : 1).

The changes in the emission curve of NCP ($c = 2 \times 10^{-5} \text{M}$) at different time intervals by the addition of OCl^- ($c = 2 \times 10^{-4}$) and calculation of the first-order rate constant:

Fig. S6 represents the changes in the emission intensity at different time intervals by the addition of hypochlorite. From the time vs. fluorescent intensity plot at a fixed wavelength of 438 nm using the first-order rate equation, we get the rate constant $K = \text{slope} \times 2.303 = 11.807 \times 2.303 = 27.192 \text{ Sec}^{-1}$

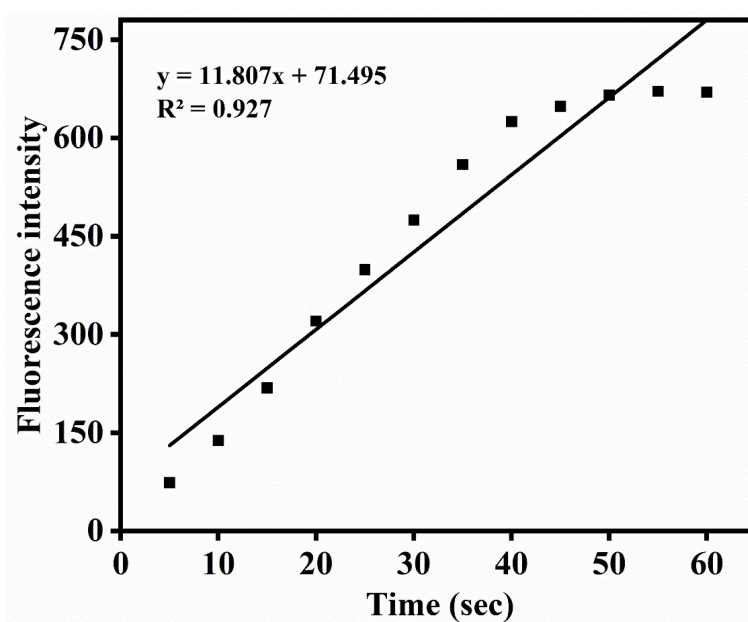


Fig. S6. First-order rate equation using time vs. fluorescent intensity plot at 438 nm.

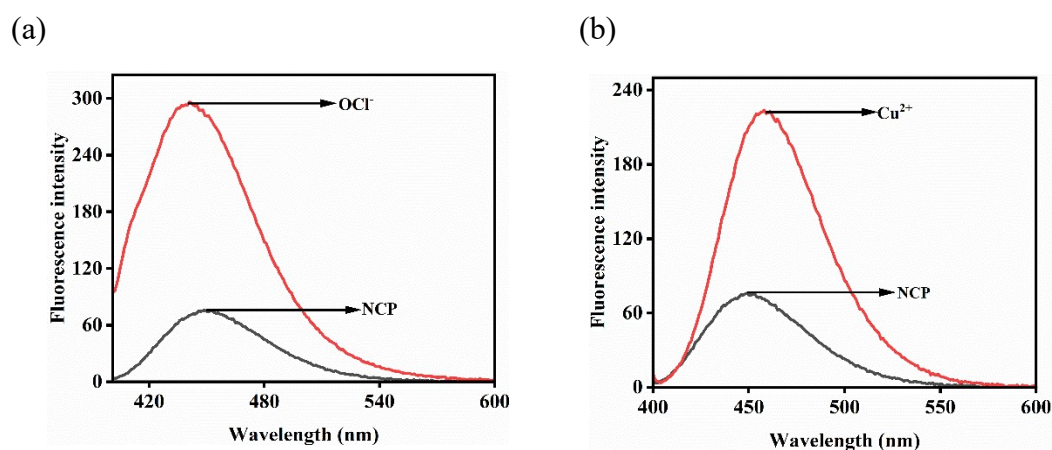
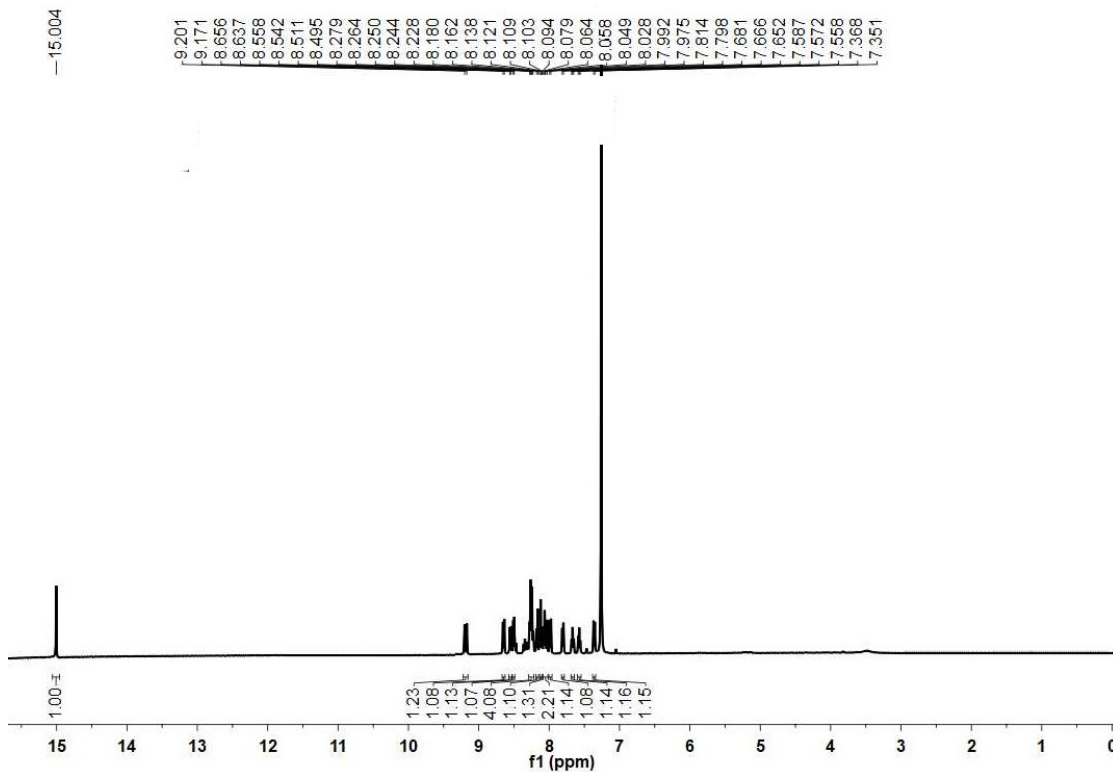
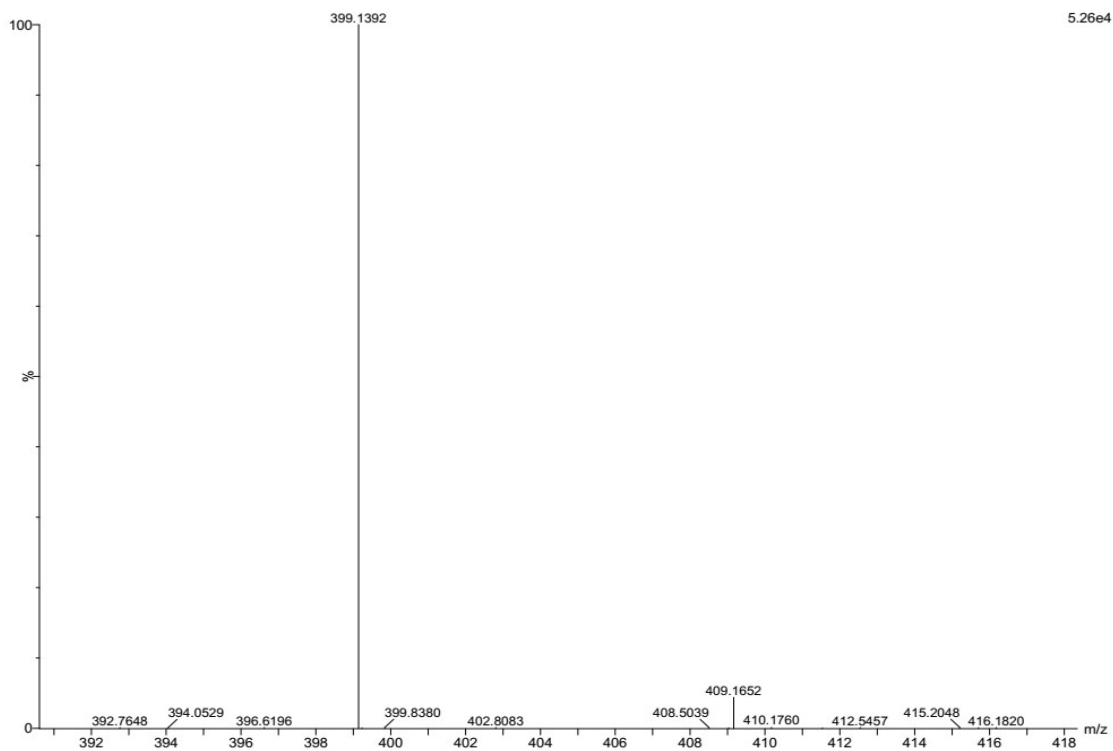


Fig. S7. (a) and (b) Fluorescence titration spectra of NCP ($c = 2.0 \times 10^{-5} \text{M}$) in the presence of OCl^- and Cu^{2+} respectively ($c = 2.0 \times 10^{-4} \text{M}$) in a $\text{CH}_3\text{CN}/\text{HEPES}$ buffer (50 : 50, v/v, pH 7.4).

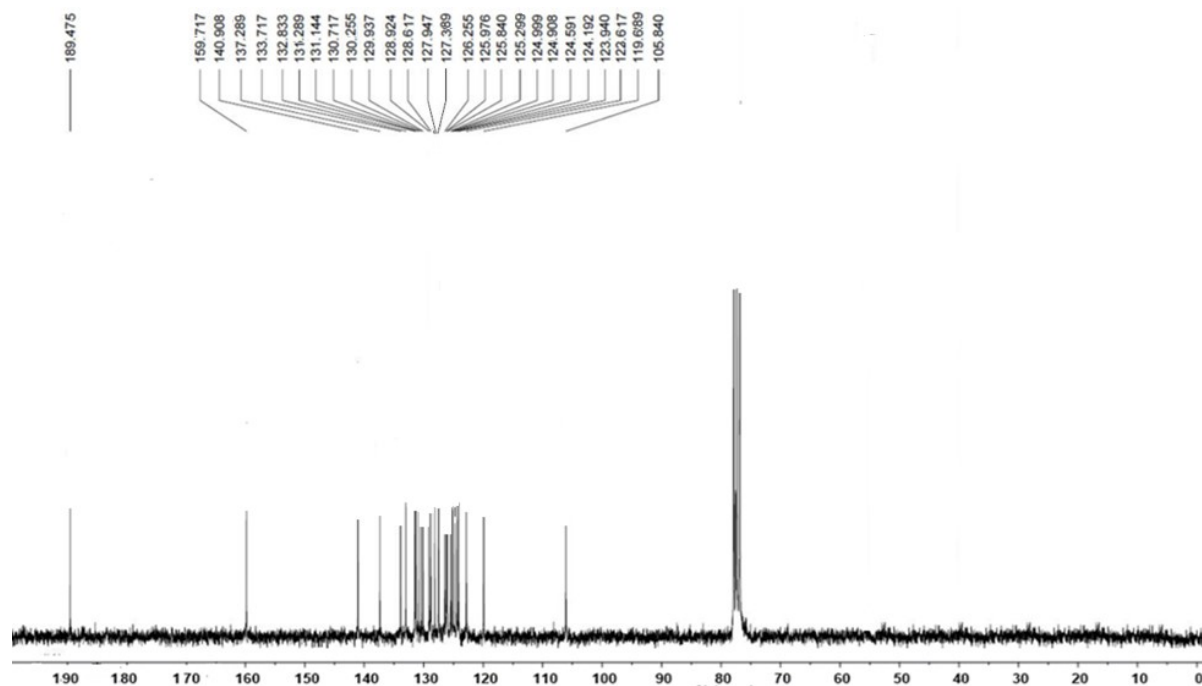
¹H NMR spectrum (Fig. S8) of NCP:



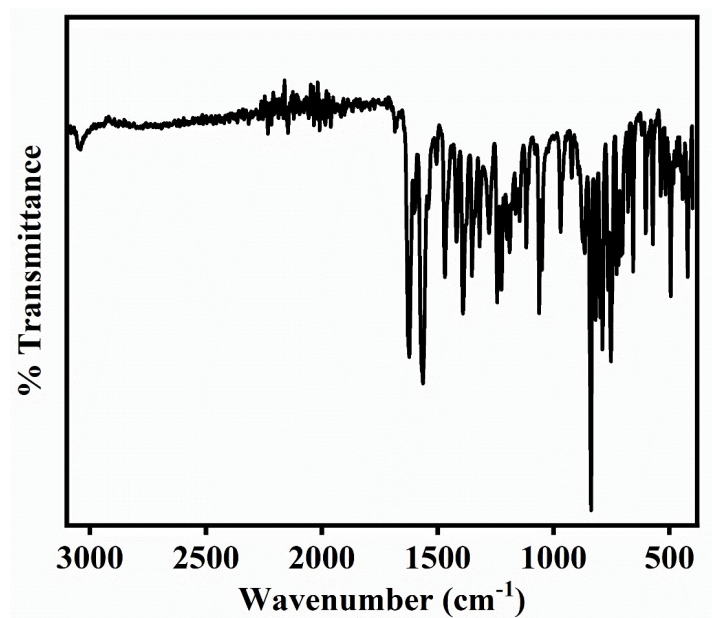
Mass spectrum (Fig. S9) of NCP:



^{13}C -NMR spectrum (Fig. S10) of NCP:



IR spectrum of NCP (Fig. S11):



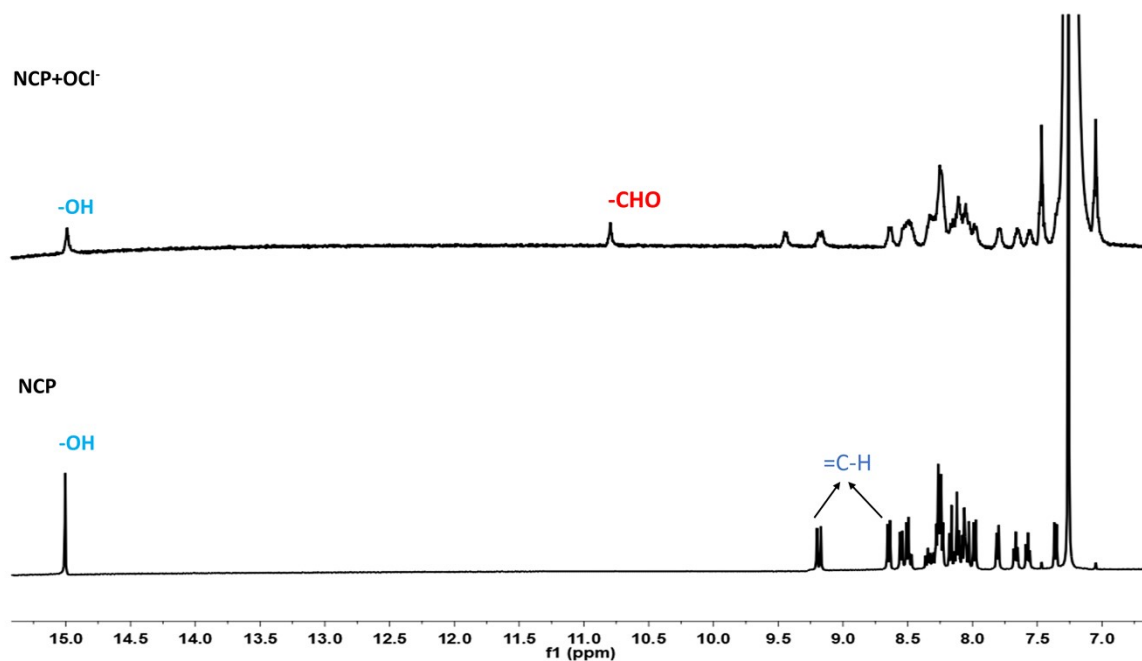


Fig. S12. ¹H-NMR analysis of NCP and NCP + OCl⁻.

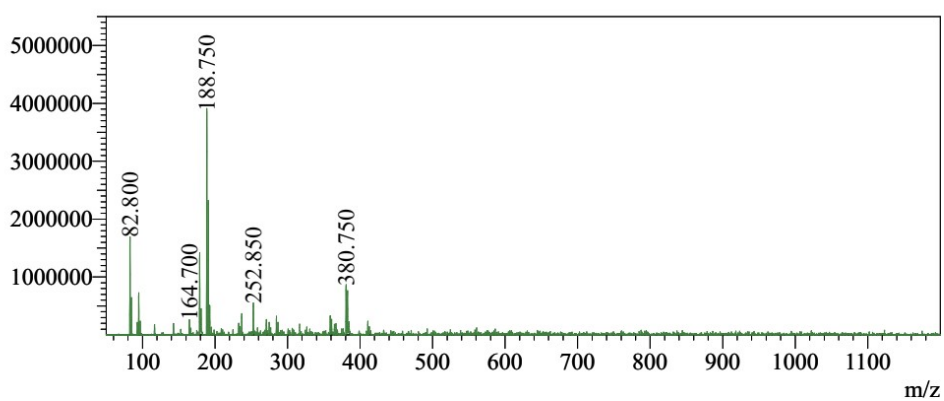


Fig. S13. Mass spectra of NCP + OCl⁻.

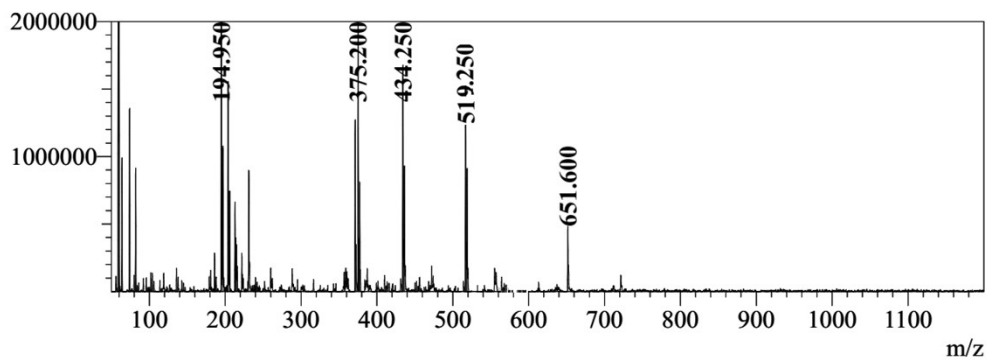


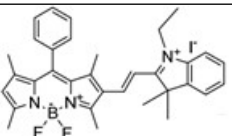
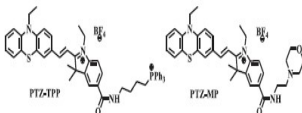
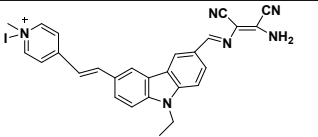
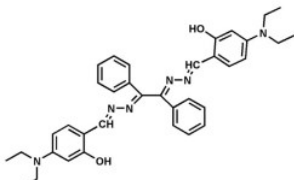
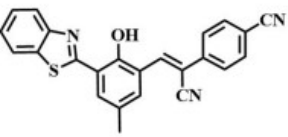
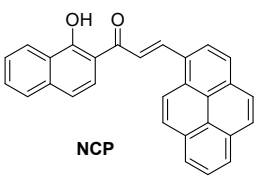
Fig. S14. Mass spectra of NCP + Cu²⁺.

Computational details

Ground-state electronic structure calculations in the gas phase of the complexes were carried out using the DFT¹ method associated with the conductor-like polarizable continuum model (CPCM).² Becke's hybrid function³ with the Lee-Yang-Parr (LYP) correlation function⁴ was used for the study. The absorbance spectral properties in a DMSO medium for **HL** and **1** were calculated by the time-dependent density functional theory (TDDFT)⁵ associated with the conductor-like polarizable continuum model and we computed the lowest 40 singlet – singlet transition.

For H atoms, we used the 6-31+(g) basis set; for C, N, O, and Cu atoms, we employed LanL2DZ as the basis set for all the calculations. The calculated electron-density plots for frontier molecular orbitals were prepared using the Gauss View 5.1 software. All the calculations were performed using the Gaussian 09W software package.⁶ The Gauss Sum 2.1 program⁷ was used to calculate the molecular orbital contributions from groups or atoms.

Table S1: Comparison table of **NCP** with the reported similar types of chemosensors

Ligands	Analytes	Solvent used	Probe type	Detection limit	Applications	References
	OCl ⁻ and viscosity	CH ₃ CN-H ₂ O (Sensing) Glycerol (Viscosity)	Turn on	28 nM	Cell imaging	[8]
	OCl ⁻ and viscosity	H ₂ O (Sensing) glycerol (Viscosity)	Turn on	19.4 nM	Cell imaging	[9]
	OCl ⁻ and Cu ²⁺	DMSO/PBS, CH ₃ CN/PBS buffer	Turn on	0.44 μM	Cell imaging	[10]
	OCl ⁻ and Cu ²⁺	CH ₃ CN-H ₂ O	Turn on	-	Logic gates	[11]
	OCl ⁻ and AIE	DMF-H ₂ O	Turn on	0.39 μM	Cell imaging	[12]
	OCl ⁻ and Cu ²⁺ , AIE, viscosity	CH ₃ CN-H ₂ O (Sensing and AIE) Glycerol (Viscosity)	Turn on	3.97 μM (Cu ²⁺) and 0.55 μM (OCl ⁻)	DFT SEM Cell Imaging Dipstick method	This work

10. References:

- 1 R. G. Parr and W. Yang, *Density Functional Theory of Atoms and Molecules*, Oxford University Press, Oxford, 1989.
- 2 (a) V. Barone and M. Cossi, *J. Phys. Chem. A*, 1998, **102**, 1995; (b) M. Cossi and V. Barone, *J. Chem. Phys.*, 2001, **115**, 4708; (c) M. Cossi, N. Rega, G. Scalmani and V. Barone, *J. Comp. Chem.*, 2003, **24**, 669.
- 3 A. D. Becke, *J. Chem. Phys.*, 1993, **98**, 5648.
- 4 C. Lee, W. Yang and R. G. Parr, *Phys. Rev. B*, 1998, **37**, 785.
- 5 M. E. Casida, C. Jamorosi, K. C. Casida and D. R. Salahub, *J. Chem. Phys.*, 1998, **108**, 4439; R. E. Stratmann, G. E. Scuseria, M. J. Frisch, *J. Chem. Phys.*, 1998, **109**, 8218; R. Bauernschmitt and R. Ahlrichs, *Chem. Phys. Lett.*, 1996, **256**, 454.
- 6 M. J. Frisch, G. W. Trucks, H. B. Schlegel, G. E. Scuseria, M. A. Robb, J. R. Cheeseman, G. Scalmani, V. Barone, B. Mennucci, G. A. Petersson, H. Nakatsuji, M. Caricato, X. Li, H. P. Hratchian, A. F. Izmaylov, J. Bloino, G. Zheng, J. L. Sonnenberg, M. Hada, M. Ehara, K. Toyota, R. Fukuda, J. Hasegawa, M. Ishida, T. Nakajima, Y. Honda, O. Kitao, H. Nakai, T. Vreven, J. A. Montgomery Jr., J. E. Peralta, F. Ogliaro, M. Bearpark, J. J. Heyd, E. Brothers, K. N. Kudin, V. N. Staroverov, R. Kobayashi, J. Normand, K. Raghavachari, A. Rendell, J. C. Burant, S. S. Iyengar, J. Tomasi, M. Cossi, N. Rega, J. M. Millam, M. Klene, J. E. Knox, J. B. Cross, V. Bakken, C. Adamo, J. Jaramillo, R. Gomperts, R. E. Stratmann, O. Yazyev, A. J. Austin, R. Cammi, C. Pomelli, J. W. Ochterski, R. L. Martin, K. Morokuma, V. G. Zakrzewski, G. A. Voth, P. Salvador, J. J. Dannenberg, S. Dapprich, A. D. Daniels, Ö. Farkas, J. B. Foresman, J. V. Ortiz, J. Cioslowski and D. J. Fox, Gaussian Inc., 2009, Wallingford CT.
- 7 N. M. O'Boyle, A. L. Tenderholt and K. M. Langner, *J. Comp. Chem.*, 2008, **29**, 839.
- 8 X. Wang, F. Song and X. Peng, *Dyes Pigm.*, 2016, **125**, 89–94.
- 9 L. Liang, Y. Sun, C. Liu, X. Jiao, Y. Shang, X. Zeng, L. Zhao and J. Zhao, *J. Mol. Struct.*, 2021, **1227**, 129523.
- 10 Y. Feng, S. Li, D. Li, Q. Wang, P. Ning, M. Chen, X. Tian and X. Wang, *Sens. Actuators B Chem.*, 2018, **254**, 282–290.
- 11 X. Xie, X. Chen, B. Li and L. Zhang, *Dyes Pigm.*, 2013, **98**, 422–427.
- 12 S. Li, Y. Zeng, C. Tang, F. Wang, B. Gu and S. Tang, *Spectrochim. Acta A Mol. Biomol. Spectrosc.*, 2022, **281**, 121601.